Article

Discovery Medicine 2026; 38(205): 430–442
https://doi.org/10.24976/Discov.Med.202638205.36

The Effect of Increased HSF1-HMOX1 Expression in H9C2 Cardiomyocytes Following Hypoxia/Reoxygenation on Myocardial Ferroptosis and M1 Polarization of Macrophages

Zicheng Wang[1], Shengjie Wang[2], Da Gao[2], Liangrong Zheng[1,*]

[1]Department of Cardiology, The First Affiliated Hospital, Zhejiang University School of Medicine, 310003 Hangzhou, Zhejiang, China
[2]Department of Cardiovascular Medicine, Ningbo Medical Center Lihuili Hospital, 315040 Ningbo, Zhejiang, China
*Correspondence: 1191066@zju.edu.cn (Liangrong Zheng)
Submitted: 11 July 2025 Revised: 20 November 2025 Accepted: 27 November 2025 Published: 20 February 2026

Background: Myocardial ischemia/reperfusion injury (MIRI) remains a leading cause of morbidity and mortality in patients with cardiovascular disease. Ferroptosis, an iron-dependent form of regulated cell death, has been increasingly implicated in cardiomyocyte damage during MIRI. Heat shock factor 1 (HSF1) and heme oxygenase-1 (HMOX1) are stress-responsive proteins, but their interplay in regulating ferroptosis during myocardial injury has not been fully elucidated. This study aimed to investigate the role of the HSF1–HMOX1 axis in modulating ferroptosis and myocardial injury after ischemia/reperfusion (I/R).
Methods: An I/R rat model was established by transient ligation of the left anterior descending coronary artery, with sham-operated rats serving as controls. H9c2 cardiomyocytes subjected to hypoxia/reoxygenation (H/R) and co-cultured with RAW 264.7 macrophages were used for *in vitro* experiments. HSF1 overexpression and knockdown, as well as HMOX1 knockdown via siRNA, were performed. Myocardial injury was assessed by measurement of serum creatine kinase–myocardial band (CK-MB) and cardiac troponin I (cTn-I), as well as histologic and immunohistochemical means. Ferroptosis was evaluated using cell viability assays, reactive oxygen species (ROS) detection, and protein detection of glutathione peroxidase 4 (GPX4), SLC7A11, and ACSL4 by means of Western blotting. Inflammatory responses and macrophage polarization were analyzed by enzyme-linked immunosorbent assay (ELISA) and flow cytometry.
Results: HSF1 and HMOX1 expression were transiently upregulated in myocardial tissues during early I/R but decreased at 24 h. HSF1 overexpression further increased ROS accumulation and exacerbated ferroptosis, as reflected by GPX4 downregulation and ACSL4 upregulation. Conversely, HSF1 knockdown attenuated ferroptosis and injury. HMOX1 knockdown reversed the pro-ferroptotic effects of HSF1 overexpression, indicating that HMOX1 mediates HSF1-induced ferroptosis. Furthermore, the HSF1–HMOX1 axis promoted macrophage polarization toward the pro-inflammatory M1 phenotype, enhancing tumor necrosis factor alpha (TNF-α) and interleukin (IL)-6 secretion.
Conclusions: The HSF1–HMOX1 axis promotes ferroptosis and exacerbates myocardial damage in ischemia/reperfusion injury by integrating stress response pathways and inflammatory regulation. Inhibiting this axis may represent a promising therapeutic strategy for reducing MIRI and improving cardiac outcomes.

Keywords: ferroptosis; macrophage polarization; myocardial reperfusion injury; heat shock transcription factors; heme oxygenase-1

Introduction

Myocardial ischemia/reperfusion injury (MIRI) represent a major cause of mortality in patients with heart disease [1]. Under hypoxia/reoxygenation (H/R) conditions, the survival and function of cardiomyocytes are severely compromised, ultimately leading to cell death. Current research indicates that hypoxia triggers ferroptosis in cardiomyocytes, a novel form of regulated cell death distinct from traditional apoptosis. Ferroptosis is closely associated with intracellular iron accumulation and lipid peroxidation, rendering its impact on cardiomyocytes and subsequent immune responses a subject of intense investigation [2].

Multiple studies have explored the underlying mechanisms of ferroptosis in MIRI. For instance, sestrin 1 was found to mitigate MIRI-induced damage by regulating the antioxidant enzyme glutathione peroxidase 4 (GPX4), thereby influencing ferroptosis [3]. Furthermore, natural plant compounds such as paeoniflorin and resveratrol have demonstrated protective effects by correcting imbalances in factors associated with ferroptosis [4]. Acute myocardial infarction (AMI) involves not only direct cardiomyocyte injury but also complex inflammatory responses, in which macrophage polarization plays a critical role [5]. Studies reveal that M1 macrophages promote inflammation and exacerbate cardiac damage in the early phase, while M2

macrophages contribute to inflammation resolution and tissue repair [6]. For example, interleukin (IL)-38 was shown to alleviate MIRI by promoting the M1-to-M2 transition, inhibiting NLRP3 inflammasome activation, and enhancing the secretion of anti-inflammatory factors [7].

Evidence demonstrates that ferroptotic cardiomyocytes in myocardial infarction release exosomes, which carry activators of the Wnt/β-catenin signaling pathway promoting macrophage polarization toward the pro-inflammatory M1 phenotype (characterized by high NOS2 and low IL-10 expression), thereby exacerbating myocardial inflammation and injury [8]. Conversely, exosomes derived from cardiomyocytes treated with the ferroptosis inhibitor ferrostatin-1 reversed this effect, indicating that ferroptosis is a key determinant of exosome functionality [8]. This discovery unveils a novel mechanism whereby ferroptosis regulates the immune microenvironment via exosomes. Targeting both ferroptosis and macrophage polarization has emerged as a promising combined therapeutic strategy for myocardial infarction. In sepsis-induced myocardial injury, a nanocomposite containing ceria nanozymes (CeO_2) and curcumin (CeCH) has been shown to alleviate damage through dual actions: CeO_2 scavenges reactive oxygen species (ROS) via its superoxide dismutase (SOD)/catalase (CAT)-like activity, suppressing cardiomyocyte ferroptosis, while curcumin promotes anti-inflammatory M2 macrophage polarization, reducing pro-inflammatory cytokine release [9]. This combined strategy significantly improved cardiac function, offering a novel therapeutic approach for inflammation-related myocardial injury.

Against this backdrop, heat shock factor 1 (HSF1) and heme oxygenase-1 (HMOX1), key regulators of the hypoxic response, have garnered increasing research attention. HSF1, a transcription factor, participates in cellular stress responses by modulating cellular tolerance and survival capacity, while HMOX1 is intricately linked to iron metabolism and cytoprotection. Research has identified a mutual regulatory relationship between HSF1 and HMOX1; however, the role of this signaling axis during H/R remains insufficiently explored [10,11]. Although some studies have investigated the impact of hypoxia on cardiomyocytes, a significant knowledge gap persists regarding the relationship between the HSF1–HMOX1 pathway, cardiomyocyte ferroptosis, and macrophage polarization.

This study aims to investigate the impact of the HSF1–HMOX1 axis on ferroptosis in H9c2 cardiomyocytes under H/R conditions and its role in promoting M1 macrophage polarization. Cell culture, H/R animal models, Western blot analysis, quantitative real-time polymerase chain reaction (qPCR), ferroptosis assays, and co-culture systems were employed to systematically evaluate the relationship between HSF1–HMOX1 expression dynamics and cardiomyocyte function, and to assess the influence of ferroptotic cardiomyocytes on M1 macrophage polarization. These investigations provide deeper insights into the role of the HSF1–HMOX1 signaling pathway in cardiomyocytes and establish a theoretical foundation for future intervention strategies.

Materials and Methods

Bioinformatics Analysis

The GSE254950 dataset was retrieved from database (https://www.ncbi.nlm.nih.gov/geo/). Differential expression analysis was performed using the limma R package (version 3.40.6; Bioconductor Project, Seattle, WA, USA), which applies generalized linear models for assessing expression changes [12]. Gene expression differences between groups were assessed based on $\log_2$ fold change ($\log_2$FC) and adjusted p-values. To identify significantly differentially expressed genes (DEGs), we applied the thresholds of $|\log_2 FC| > 1.5$ and false discovery rate (FDR, Benjamini–Hochberg correction) < 0.05. This combined cutoff ensured both biological relevance and statistical rigor.

Cell Culture and Treatments

H9c2 cardiomyocytes (ATCC® CRL-1446™) were cultured in DMEM (Gibco, Cat# 11965-092; Waltham, MA, USA) supplemented with 10% fetal bovine serum (FBS; Gibco, Cat# 10099-141; Waltham, MA, USA) and 1% penicillin/streptomycin (HyClone, Cat# SV30010; Logan, UT, USA). RAW 264.7 macrophages (ATCC® TIB-71™) were maintained in RPMI-1640 (Gibco, Cat# 11875-093) with 10% FBS. For H/R modeling, cells were exposed to hypoxia (1% O_2, 5% CO_2, 94% N_2; 6 h) in a tri-gas incubator (Heracell^{TM} VIOS 160i, Thermo Scientific; Waltham, MA, USA), followed by reoxygenation (21% O_2; 12 h). H9c2 cardiomyocytes and RAW 264.7 macrophages were authenticated by short tandem repeat (STR) profiling prior to use, confirming their identity. In addition, all cell cultures were routinely tested for mycoplasma contamination by PCR-based assays (Cat. No. LT07-318, MycoAlert, Lonza; Basel, Switzerland), and results revealed negative contamination. Unless otherwise indicated, si-HSF1-1 and si-HMOX1-1 were used for all subsequent knockdown experiments; the "-2" duplexes were only used for initial validation.

H9c2 cells were transfected with siRNAs targeting HSF1 or HMOX1 using Lipofectamine RNAiMAX (Cat. No. 13778075, Thermo Fisherr; Waltham, MA, USA) according to the manufacturer's instructions. Cells were seeded the day before transfection in 6-well plates at 1.5×10^5 cells/well (≈60–70% confluence at transfection). Unless otherwise indicated, the final siRNA concentration was 50 nM in Opti-MEM (Cat. No. 31985070, Gibco; Waltham, MA, USA) and the medium was replaced with complete growth medium 6 h after transfection. A non-

targeting siRNA (si-NC) was used as a negative control in all experiments.

Two independent duplexes were designed for each gene (si-HSF1-1/-2, si-HMOX1-1/-2; sequences listed in the **Supplementary materials**). Knockdown validation was performed 24 h post-transfection by qPCR (and, where applicable, Western blotting), and duplexes achieving ≥70% mRNA reduction relative to si-NC were considered effective. Unless otherwise indicated, si-HSF1-1 and si-HMOX1-1 were used for all subsequent knockdown experiments, while "-2" duplexes were only used for initial validation (see **Supplementary Fig. 1** for the efficiency screen).

For hypoxia/reoxygenation (H/R) experiments, cells were subjected to the H/R protocol 24 h after transfection (entailing 6 h hypoxia at 1% O_2 followed by 12 h reoxygenation), and samples were collected for downstream assays 24–36 h post-transfection, such as qPCR assay, Western blotting, ROS level measurement, CCK-8 assay, and TUNEL assay. To minimize off-target effects, all knockdown experiments were performed with biological triplicates, and results were reproduced in at least two independent transfections. Data are reported as mean ± standard deviation (SD), and statistical comparisons were made against si-NC controls.

Animal Model of MIRI

This study utilized a rodent LAD ischemia/reperfusion (I/R) model established in accordance with protocols described elsewhere [13]. A total of 36 male Sprague–Dawley rats (8–10 weeks old, each weighing 200–250 g; Vital River, Beijing, China) were used in this study. The animals were randomly divided into six groups: the Sham group, I/R 6 h, I/R 12 h, I/R 24 h, I/R + KRIBB11, and I/R + AAV9-HMOX1 groups. MIRI was established by transient ligation of the left anterior descending coronary artery (LAD) for 30 minutes, followed by reperfusion as previously described. The Sham group underwent the same surgical procedures without LAD ligation.

For the time-course experiments in the Sham, I/R 6 h, I/R 12 h, and I/R 24 h groups, hearts were collected at the corresponding reperfusion time points to observe the dynamic changes of myocardial injury and ferroptosis. For the intervention experiments in the I/R + KRIBB11 and I/R + AAV9-HMOX1 groups, the reperfusion time was fixed at 12 hours, which represented the peak of myocardial injury observed in the time-course analysis. The HSF1 inhibitor KRIBB11 (5 mg/kg; MedChemExpress, HY-119374) was administered via tail-vein injection once daily for three consecutive days before I/R surgery. The AAV9-HMOX1 vector (1×10^{11} vg in 200 µL PBS; HanBio) was delivered by tail-vein injection two weeks before I/R to achieve effective cardiac transduction.

At each time point, six rats were included per group. Of these, three animals were used for histological and immunohistochemical analyses (TTC, Masson, and CD68/CD206 staining), and the remaining three were used for molecular and biochemical assays (Western blotting, qPCR, and ELISA). This sampling design minimized biological variation and avoided repeated freeze–thaw cycles of tissue samples.

Rats were anesthetized with isoflurane—induced at 4–5% in 100% O_2 (1.0–1.5 L/min) and maintained at 1.5–2.0% via a nose cone throughout surgery; anesthetic depth was monitored by pedal withdrawal reflex and respiratory rate, and body temperature was maintained at 37.0 ± 0.5 °C with a thermostatic heating pad. After reperfusion, hearts were excised, rinsed with cold saline, and processed for either fixation in 4% paraformaldehyde or snap-freezing in liquid nitrogen. At the end of the experiment, animals were humanely euthanized with intraperitoneal administration of sodium pentobarbital (≥150 mg/kg).

All animal experiments were approved by the Animal Ethics Committee of the First Affiliated Hospital, Zhejiang University School of Medicine (Approval No. 20240146) and conducted in accordance with institutional and ARRIVE guidelines.

Cellular and Molecular Assays

Flow Cytometry Analysis of Macrophage Polarization

RAW 264.7 macrophages were harvested after coculture and washed twice with phosphate-buffered saline (PBS). The cells were incubated with fluorochrome-conjugated antibodies against CD86 (M1 marker) and CD206 (M2 marker) (BioLegend, San Diego, CA, USA) for 30 min at 4 °C in the dark. After washing, the cells were analyzed using a BD FACSCanto II flow cytometer (3-laser configuration 405/488/633 nm, BD Biosciences, Franklin Lakes, NJ, USA). Data were processed using FlowJo software (v10.7.1, Tree Star, Ashland, OR, USA), and the percentages of $CD86^+$ and $CD206^+$ subsets were quantified from three independent experiments.

Immunohistochemistry (IHC)

Paraffin-embedded myocardial tissue sections (5 µm) were deparaffinized, rehydrated, and subjected to antigen retrieval in citrate buffer (pH 6.0) using microwave heating. Endogenous peroxidase activity was quenched with 3% H_2O_2 for 10 min. After blocking with 5% normal goat serum (ZSGB-BIO, Cat# ZLI-9022; Beijing, China), sections were incubated overnight at 4 °C with primary antibodies against CD68 (Abcam, ab125212, rabbit monoclonal, 1:200) and CD206 (Abcam, ab64693, rabbit polyclonal, 1:200).

The next day, the sections were washed and incubated with goat anti-rabbit IgG (H+L), HRP-conjugated secondary antibody (ZSGB-BIO, Cat# ZB-2301, 1:500; Beijing, China) for 1 h at room temperature. Staining was visualized using a DAB Substrate Kit (Vector Laboratories, Cat# SK-4100) and counterstained with hematoxylin (Be-

yotime, Cat# C0107). Images were acquired with a Nikon Eclipse Ci-L microscope, and positive staining was quantified using ImageJ software (v1.53, NIH, Bethesda, MD, USA).

Western blotting

Protein lysates were extracted from cells or myocardial tissue using RIPA buffer (Lot No. 20250108, Beyotime, Shanghai, China) containing protease and phosphatase inhibitors. Protein concentrations were measured with a BCA kit (Lot No. 20250112, Thermo Scientific, Waltham, MA, USA). Equal amounts of protein (20–30 µg) were separated by SDS-PAGE and transferred to PVDF membranes (Lot No. 20241218, Millipore, Burlington, MA, USA). After blocking with 5% non-fat milk, membranes were incubated overnight at 4 °C with primary antibodies against GPX4 (Abcam, Cat# ab125066, 1:1000), SLC7A11 (SLC7A11/xCT; Abcam, Cat#ab307601, 1:1000), ACSL4 (Abcam, Cat# ab155282, 1:1000), HSF1 (Cell Signaling Technology, Cat# 4356, 1:1000), and HMOX1 (Abcam, Cat# ab13243, 1:1000). β-Actin (Abcam, Cat# ab8226, 1:5000) served as the loading control.

The next day, membranes were incubated with species-appropriate HRP-conjugated secondary antibodies for 1 h at room temperature: goat anti-rabbit IgG (H+L), HRP-conjugated (Cell Signaling Technology, Cat# 7074, 1:5000); goat anti-mouse IgG (H+L), HRP-conjugated (Cell Signaling Technology, Cat# 7076, 1:5000). Protein bands were visualized using an ECL kit (Thermo Scientific, Cat# 32106; Waltham, MA, USA) on a Bio-Rad ChemiDoc Imaging System (Image Lab™ Software v6.1, Hercules, CA, USA), and densitometry was performed with ImageJ software (v1.53, NIH, Bethesda, MD, USA).

Reactive Oxygen Species (ROS) Detection

Intracellular ROS levels were detected using fluorescent probe 2′,7′-dichlorodihydrofluorescein diacetate (DCFH-DA; Beyotime, China). H9c2 cells were incubated with 10 µM DCFH-DA for 30 min at 37 °C in the dark. After washing with serum-free medium, fluorescence images were acquired with a Leica DMi8 fluorescence microscope, and mean fluorescence intensity (MFI) was quantified using ImageJ software (v1.53, NIH, Bethesda, MD, USA).

Enzyme-Linked Immunosorbent Assay (ELISA)

Serum samples from rats and cell culture supernatants were collected and centrifuged at 3000 rpm for 10 min at 4 °C. The levels of tumor necrosis factor alpha (TNF-α), IL-6, IL-10, transforming growth factor beta (TGF-β) (MultiSciences, Hangzhou, China; Cat# EK282HS, EK206, EK210, EK981EGA, respectively), creatine kinase–myocardial band (CK-MB; Elabscience, Wuhan, China, E-EL-R1327), and cardiac troponin I (cTnI; Life Diagnostics, West Chester, PA, USA, CTNI-2-US) were measured using commercial ELISA kits following the manufacturer's instructions. Absorbance was read at 450 nm using a microplate reader (BioTek Synergy™ H1, BioTek, Winooski, VT, USA). Standard curves were generated for each assay, and cytokine concentrations were calculated accordingly. Each experiment was performed in triplicate.

Platelet-Derived Growth Factor (PDGF) Measurement

PDGF levels in the cardiomyocyte-macrophage co-culture supernatants were quantified using a commercial ELISA kit (R&D Systems; Minneapolis, MN, USA. Cat. No. DY220) according to the manufacturer's instructions. Briefly, supernatants were collected after 24 h co-culture, centrifuged to remove cellular debris, and analyzed in triplicate. Absorbance was read at 450 nm using a microplate reader (BioTek Synergy™ H1, BioTek; Winooski, VT, USA), and PDGF concentrations were calculated from standard curves.

Macrophage Polarization Studies

H9c2 cells subjected to H/R ± interventions were co-cultured with RAW 264.7 macrophages in Transwell inserts (0.4 µm; Corning) for 24 h. Macrophages were stained with APC-anti-CD86 (BioLegend 105012; 1:100), PE-anti-CD80 (BioLegend 104708; 1:100) for M1 identification, or FITC-anti-CD206 (BioLegend 141704; 1:100)/PE-anti-Arg1 (Santa Cruz sc-271430; 1:100) for M2 identification, then analyzed by flow cytometry (BD FACSCanto II). TNF-α, IL-6, IL-10, and TGF-β in supernatants were quantified using ELISA kits (Lot No. 20250110, R&D Systems, Minneapolis, MN, USA). Co-culture setup and cell densities. For indirect co-culture, H9c2 cardiomyocytes were seeded into the lower chamber of 12-well plates at 2.0×10^5 cells/well ($\approx 5.0 \times 10^4$ cells/cm^2) one day before induction of H/R. After H/R interventions, Transwell inserts with 0.4 µm pores (Corning) were placed, and RAW 264.7 macrophages were seeded into the upper chamber (insert) at 1.0×10^5 cells/insert ($\approx 2.5 \times 10^4$ cells/cm^2). Co-culture was maintained for 24 h under 2% FBS to minimize proliferation-related confounding, with 1.0 mL medium remaining in the lower chamber and 0.5 mL in the upper chamber. To ensure uniform cell distribution, cell suspensions were added centrally to the well/insert, and the plates were gently rocked for ~30 s before incubation.

Histology and Immunostaining

At 24 h after reperfusion, the rats were re-anesthetized and their hearts were rapidly excised, rinsed in cold saline, and frozen at –20 °C for 20 min. The left ventricle was cut into 5–6 transverse slices (2 mm thick) from apex to base. Slices were incubated in 2% 2,3,5-triphenyltetrazolium chloride (TTC; Sigma-Aldrich, Cat# T8877) in phosphate-

Table 1. Primer sequences.

Gene	Forward (5′→3′)	Reverse (5′→3′)
HSF1	GGACATAAAAATACGCCAGGAC	GAGCTTGTTGACAACTTTTTGC
HMOX1	CAGGTGTCCAGGGAAGGCTTTAAG	TGGGTTCTGCTTGTTTCGCTCTATC
GAPDH	TGTGTCCGTCGTGGATCTGA	CCTGCTTCACCACCTTCTTGA

HSF1, Heat shock factor 1; *HMOX1*, heme oxygenase-1; *GAPDH*, glyceraldehyde-3-phosphate dehydrogenase.

buffered saline (PBS, pH 7.4) at 37 °C for 20 min in the dark, followed by fixation in 4% paraformaldehyde for 24 h.

Viable myocardium was stained red, whereas infarcted tissue remained pale white. Images were captured using a Leica DMi8 inverted microscope (Leica Microsystems, Wetzlar, Germany). The infarct area (IA), area at risk (AAR), and left ventricle (LV) area were quantified using ImageJ software. Infarct size was expressed as IA/AAR (%) and normalized to LV area when appropriate.

For additional protein expression analysis, Western blotting was performed using primary antibodies including HSF1 (Cell Signaling Technology, Cat# 4356, rabbit monoclonal, 1:1000, validated for mouse/human). HRP-conjugated goat anti-rabbit IgG (Cell Signaling Technology, Cat# 7074, 1:5000) was applied as the secondary antibody.

RNA Extraction and qPCR

Total RNA was extracted from myocardial tissue and cultured cells using TRIzol reagent (Invitrogen, Cat# 15596026). RNA concentration and purity were measured with a NanoDrop 2000 spectrophotometer (Thermo Scientific, Waltham, MA, USA). Complementary DNA (cDNA) was synthesized using the PrimeScript RT Reagent Kit (Takara, Cat# RR037A; Kusatsu, Japan) according to the manufacturer's protocol.

qPCR was performed using TB Green® Premix Ex Taq II (Takara, Cat# RR820A; Kusatsu, Japan) on an ABI StepOnePlus Real-Time PCR System (StepOnePlus™ Software v2.3, Applied Biosystems; Waltham, MA, USA). Each reaction contained 2 µL of cDNA, 10 µL of 2× TB Green mix, 0.4 µL of forward and reverse primers (10 µM), and nuclease-free water to a final volume of 20 µL. Amplification was achieved using the protocol as follows: 95 °C for 30 s, followed by 40 cycles of 95 °C for 5 s and 60 °C for 30 s. Relative gene expression levels were calculated using the $2^{-\Delta\Delta Ct}$ method, with GAPDH as the internal reference. Primer sequences are listed in Table 1. All primers were synthesized by Sangon Biotech (Shanghai, China).

Transwell Migration

For migration assays, RAW 264.7 cells (1×10^5) were seeded in serum-free medium into Transwell upper chambers (8 µm pores; Corning). Conditioned medium from H9c2 cells post-H/R, with or without interventions, was added to the lower chamber. After 24 h, migrated cells were fixed, stained with crystal violet, and counted in five random fields/membrane. For migration assays using 8 µm inserts, RAW 264.7 cells were seeded in the upper chamber at 1.0×10^5 cells/insert in serum-free medium; the lower chamber contained 600 µL of conditioned medium from H9c2 cells post-H/R ± interventions supplemented with 10% FBS as chemoattractant. After 24 h, migrated cells on the underside of the membrane were fixed, stained with crystal violet, and counted in five non-overlapping fields per membrane at 200× magnification.

Statistical Analysis

All data are presented as mean ± SD. Statistical analyses were performed using GraphPad Prism 9.0 software (GraphPad Software, San Diego, CA, USA). Comparisons between two groups were conducted using an unpaired Student's *t*-test, while comparisons among multiple groups were performed using one-way analysis of variance (ANOVA) followed by Tukey's post hoc test. A $p < 0.05$ was considered statistically significant.

Results

Transcriptomic Alterations in H/R-Treated Cardiomyocytes

To identify key genes potentially regulating H/R injury, we downloaded the GSE254950 dataset from GEO and established an H/R injury model using rat H9c2 cardiomyocytes. RNA sequencing analysis revealed the differential expression profile post-H/R (Fig. 1A,B). Compared to the controls, the H/R group exhibited 1598 upregulated and 3970 downregulated genes ($|\log_2 FC| > 1.5$, $p < 0.05$, Fig. 1A,B). Gene Ontology (GO) and Kyoto Encyclopedia of Genes and Genomes (KEGG) enrichment analyses indicated that these differentially expressed genes (DEGs) were primarily involved in DNA repair, spindle organization, and helicase activity, and enriched in pathways such as Cell cycle, DNA replication, and Mismatch repair (Fig. 1C,D). Notably, *HMOX1* expression was significantly elevated in the H/R group versus controls (Fig. 1E).

Activation of Ferroptosis in a Rat Myocardial I/R Model

In a rat ischemia/reperfusion (I/R) model, infarct size progressively increased within 24 h after 30 min ischemia

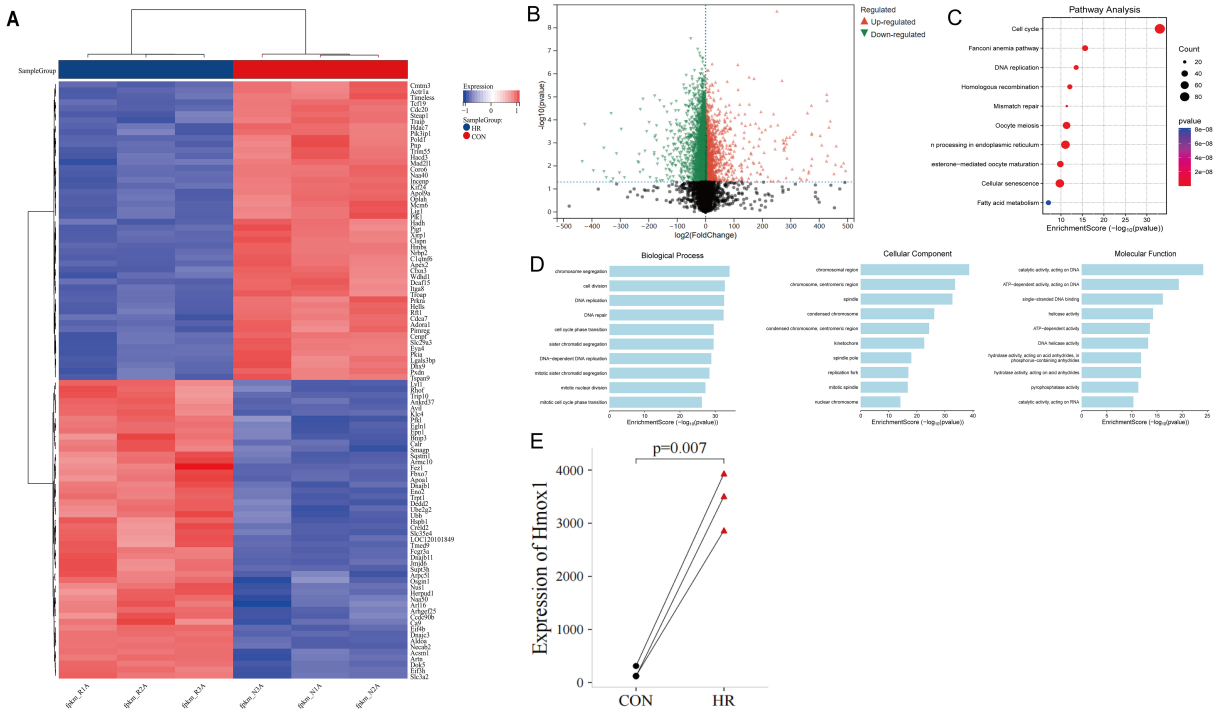

Fig. 1. Differential gene expression analysis of rat H9C2 cardiomyocytes after hypoxia/reoxygenation. (A) Heatmap of differential analysis. (B) Volcano plot of differential analysis. (C) KEGG analysis of differential genes. (D) GO analysis of differential genes. (E) Expression analysis of *Hmox1*. KEGG, Kyoto Encyclopedia of Genes and Genomes; GO, Gene Ontology.

(Fig. 2A,B). ELISA showed that serum levels of injury biomarkers CK-MB and cTn-I peaked at 12 h post-I/R ($p < 0.05$) but declined at 24 h, likely due to extensive cardiomyocyte death (Fig. 2C,D). Therefore, subsequent mechanistic experiments mainly focused on the 12 h reperfusion point, which represented the peak of myocardial injury and ferroptosis activation. Given that HMOX1 is transcriptionally regulated by HSF1, we measured their expression: both HSF1 and HMOX1 significantly increased at 0–12 h post-I/R but decreased at 24 h, aligning with CK-MB/cTn-I trends (Fig. 2E). ROS levels surged at 6 h and 12 h post-I/R ($p < 0.05$, Fig. 2G). Western blotting revealed decreased expression of anti-ferroptotic proteins (GPX4, SLC7A11) and increased pro-ferroptotic ACSL4 during reperfusion, inversely correlating with GPX4 (Fig. 2F). These changes indicate that the antioxidant defense system against lipid peroxidation was impaired, while lipid metabolic pathways driving ferroptosis were activated, thereby exacerbating myocardial injury. These results indicate that ferroptosis accompanies I/R injury and likely contributes to its pathogenesis.

HSF1 and HMOX1 are Upregulated During I/R Injury

It was noted that macrophage polarization is linked to the progression of ischemia-reperfusion injury; therefore, we validated the polarization of macrophages after myocardial I/R induction in the rats. The results showed that after the ischemia-reperfusion modeling, the number of M1-type macrophages in the heart area significantly increased, accompanied by a decrease in the proportion of M2 macrophages ($p < 0.05$) (Fig. 3A–C). This suggests that I/R creates a pro-inflammatory microenvironment dominated by M1 macrophages, which likely amplifies tissue damage through the release of TNF-α and IL-6, while limiting reparative processes mediated by M2 macrophages. We used ELISA to examine the levels of pro-inflammatory factors like TNF-α and IL-6, as well as anti-inflammatory factors like IL-10 and TGF-β in the heart tissue, revealing an increase in pro-inflammatory factors and a decrease in anti-inflammatory factors, consistent with the trend of macrophage polarization (Fig. 3D). Immunohistochemical analysis of macrophage density in the infarcted area showed a significant increase in $CD68^+$ cell numbers (Fig. 3E). Further Western blotting analysis of signaling pathways related to macrophage polarization, NF-κB and STAT3/STAT6 activation states revealed significant activation of pathways associated with M1 macrophage polarization (Fig. 3F). These results suggest that during cardiac I/R in rats, macrophages undergo M1 polarization, which may exacerbate IR injury by releasing pro-inflammatory factors. It is worth noting that flow cytometry revealed only modest changes in M1/M2 subsets under certain conditions. This likely reflects the dynamic and heterogeneous nature of macrophage polarization during reperfusion, where transitional phenotypes may coexist. Nevertheless, the trend

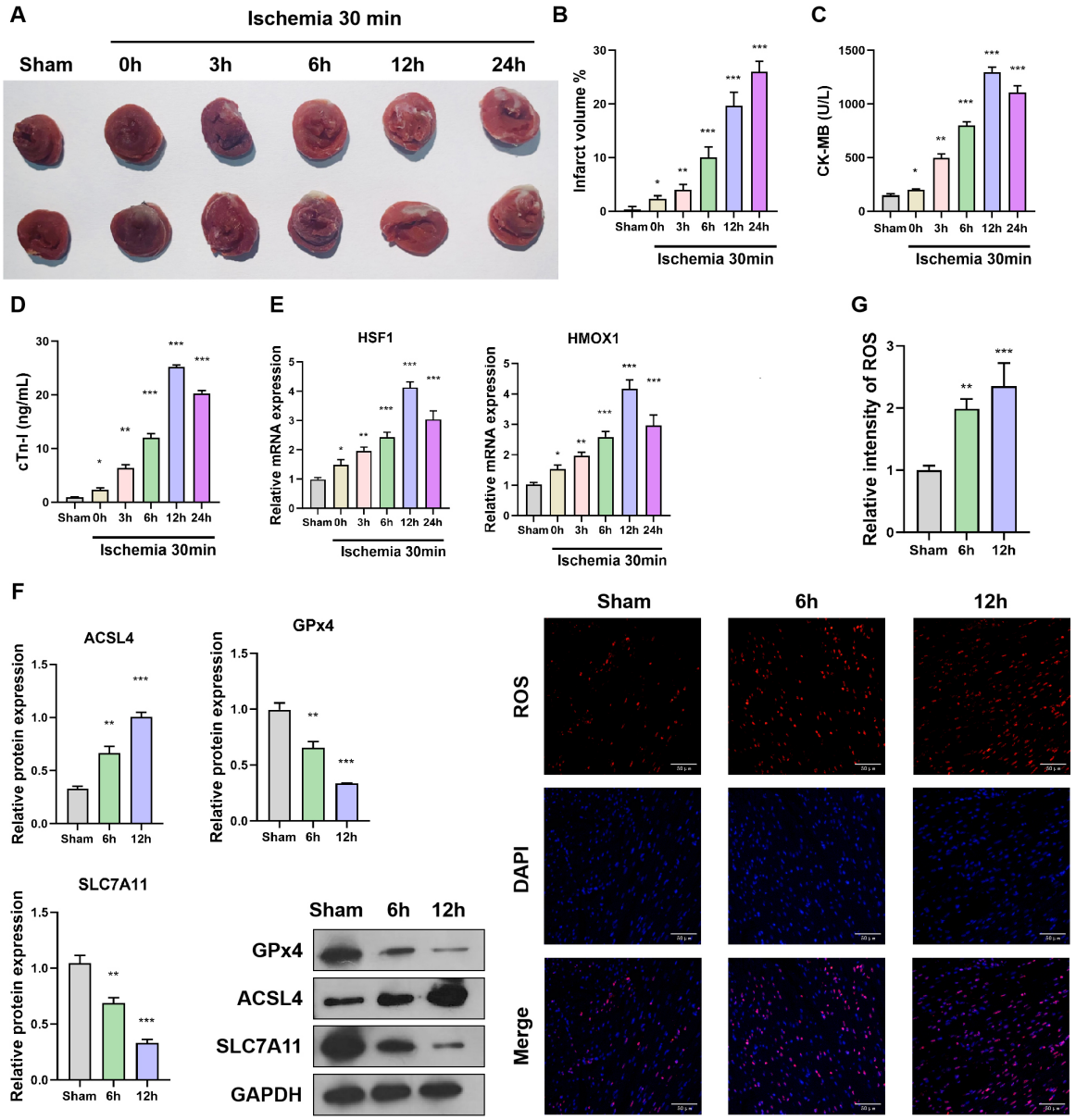

Fig. 2. Enhanced ferroptosis and HSF1/HMOX1 upregulation in rat myocardial I/R model. (A,B) TTC-stained heart sections and quantitative analysis. (C,D) CK-MB and cTn-I levels by ELISA. (E) HSF1 and HMOX1 mRNA by qPCR. (F) Detection of ferroptosis-related proteins by Western blotting. (G) ROS detection, Scale bar = 50 µm. Quantitative data are expressed as mean ± SEM (n = 6 per group); *$p < 0.05$, **$p < 0.01$, ***$p < 0.001$ vs. Sham group. HSF1, Heat shock factor 1; HMOX1, heme oxygenase-1; I/R, ischemia/reperfusion; TTC, 2,3,5-triphenyltetrazolium chloride; CK-MB, creatine kinase–myocardial band; cTn-I, cardiac troponin I; ELISA, enzyme-linked immunosorbent assay; qPCR, quantitative real-time polymerase chain reaction; ROS, reactive oxygen species; SEM, standard error of the mean.

was consistent with our cytokine analysis and immunohistochemical results, supporting an overall M1-skewed inflammatory response.

HSF1-HMOX1 Axis Regulates Cardiomyocyte Ferroptosis

To investigate whether the HSF1–HMOX1 axis regulates ferroptosis in I/R, we overexpressed HSF1 in cardiomyocytes. This reduced GPX4 and increased ACSL4 expression (Fig. 4A) and elevated ROS levels. HMOX1 knockdown reversed these effects (Fig. 4B–D). CCK-8 and TUNEL assays confirmed that HSF1 overexpression significantly decreased cell viability ($p < 0.05$), while HMOX1 silencing restored viability to near-control levels ($p < 0.05$) (Fig. 4E). Thus, HSF1 likely promotes ferroptosis by regulating HMOX1.

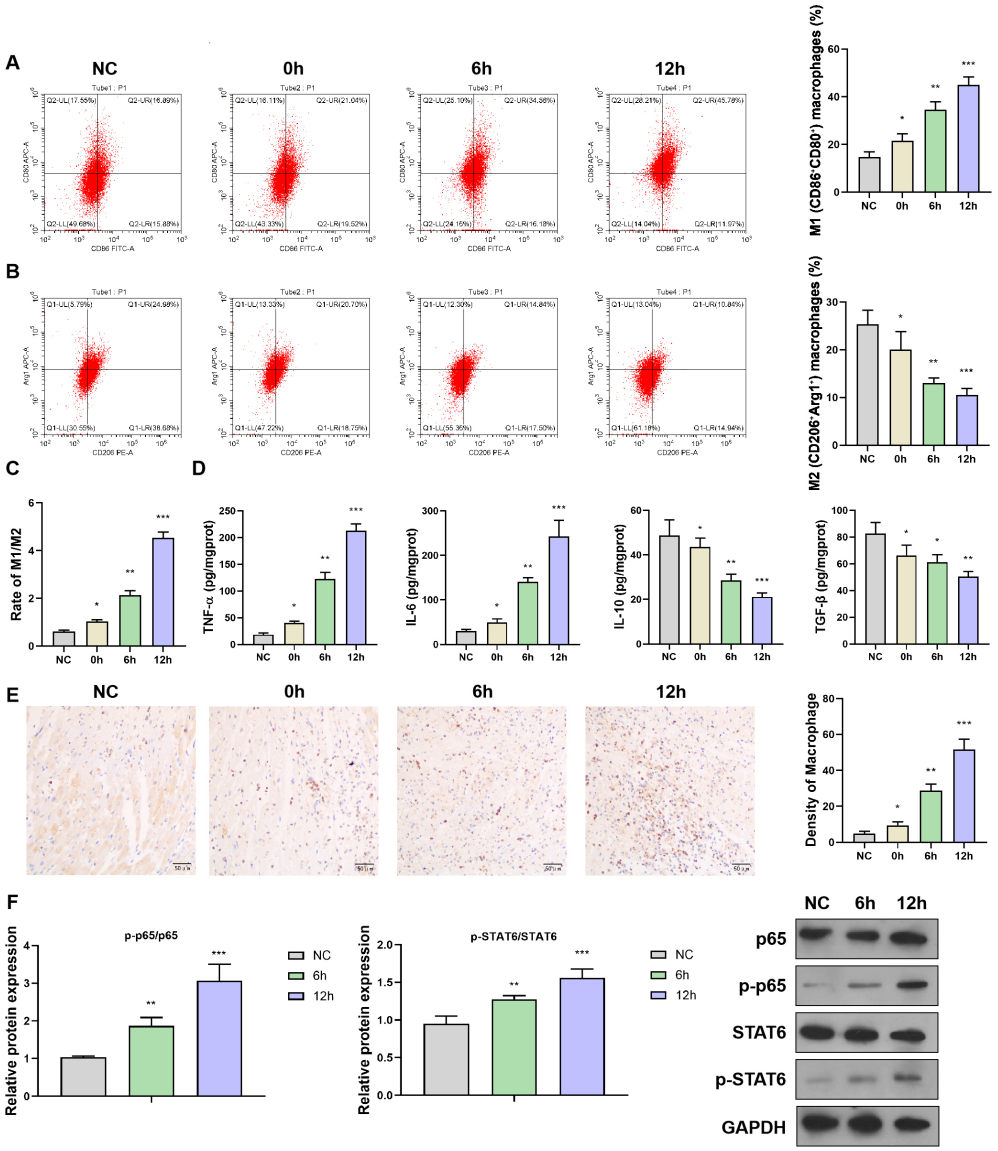

Fig. 3. Macrophages shift toward M1 polarization after myocardial ischemia-reperfusion in rats. (A–C) Flow cytometry analysis of macrophage polarization status after myocardial infarction. (D) ELISA detection of dynamic expression of pro-inflammatory (TNF-α, IL-6) and anti-inflammatory (IL-10, TGF-β) cytokines in myocardial tissue. (E) Immunohistochemical detection of macrophage density in the infarcted area (scale bar = 50 µm). (F) Western blot analysis of macrophage polarization-related signaling pathways to measure activation of NF-κB (p-p65/p65) and STAT6 (p-STAT6/STAT6). $n = 3$ per group; *$p < 0.05$, **$p < 0.01$, ***$p < 0.001$ vs. NC. TNF-α, tumor necrosis factor alpha; IL, interleukin; TGF-β, transforming growth factor beta; NF-κB, nuclear factor kappa-light-chain-enhancer of activated B cells; STAT6, signal transducer and activator of transcription 6; NC, negative control.

Impact of Cardiomyocyte Ferroptosis on Macrophage Polarization

In a cardiomyocyte-macrophage co-culture system, HSF1-HMOX1 knockdown increased M2 macrophages ($p < 0.05$) (CD206+/Arg1+) and decreased M1 subsets ($p < 0.05$) (CD86+/CD80+), while overexpression promoted M1 polarization ($p < 0.05$) (Fig. 5A). Transwell assays showed enhanced macrophage migration toward HSF1-overexpressing cardiomyocytes (Fig. 5B). ELISA revealed elevated TNF-α/IL-6 and reduced TGF-β/PDGF in co-culture supernatants after HSF1 activation (Fig. 5C). This cytokine profile is consistent with enhanced M1 polarization and suppressed M2-mediated repair, highlighting that cardiomyocyte ferroptosis indirectly regulates macrophage functional states. Western blotting confirmed that the si-HSF1 group exhibited reduced p-p65 and increased p-Smad3 signaling (Fig. 5D) compared with the control group. These results demonstrate that the HSF1–HMOX1 axis drives M1 polarization by inducing cardiomyocyte ferroptosis.

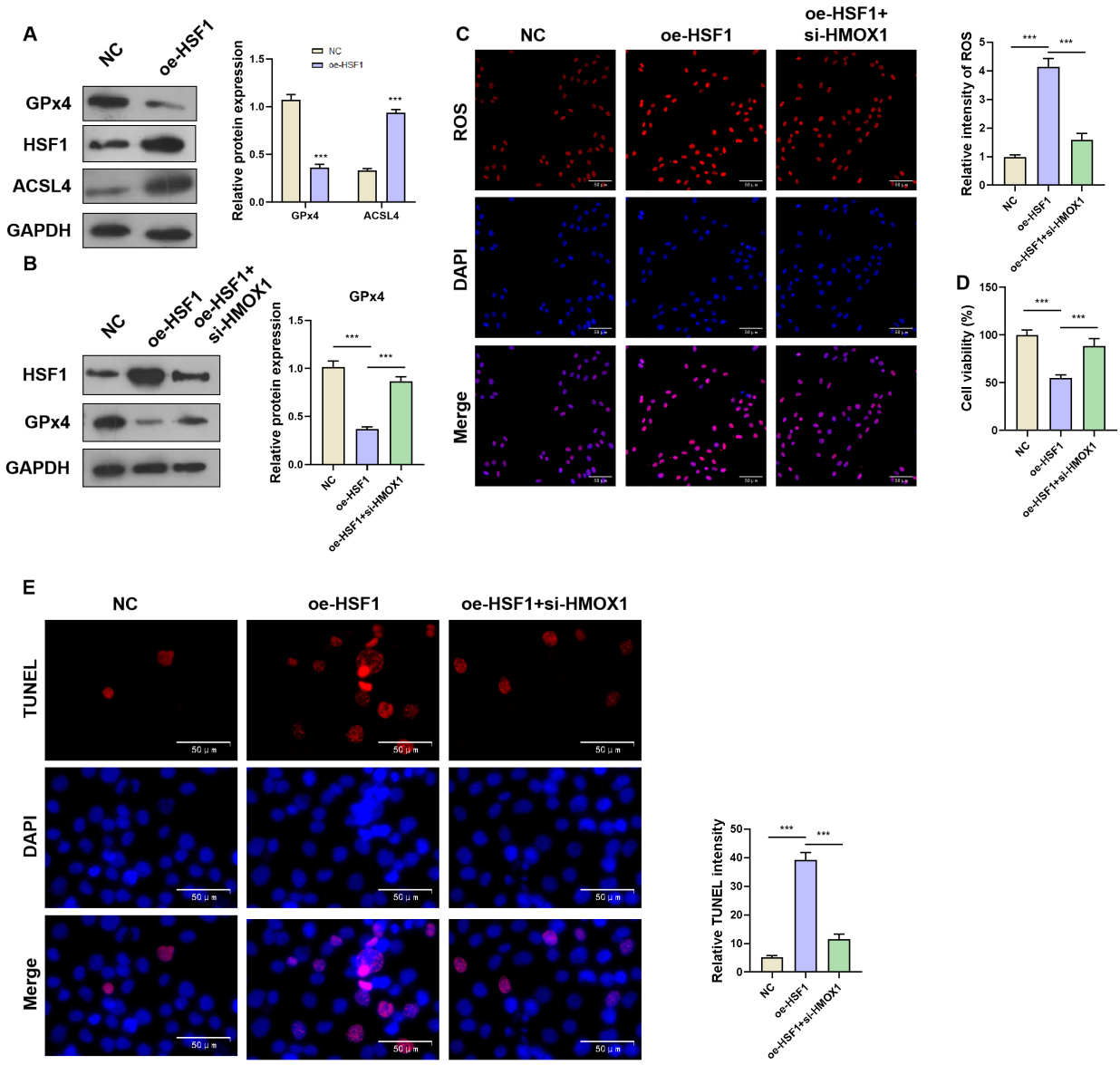

Fig. 4. The HSF1–HMOX1 Axis Promotes Ferroptosis in Cardiomyocytes. (A) Western blot detection of ferroptosis-related proteins in cardiomyocytes. (B) Detection of ferroptosis markers after HSF1 overexpression and HMOX1 knockdown (qPCR validation results of si-HMOX1 efficiency is shown in **Supplementary Fig. 1**). (C) Measurement of ROS levels after HSF1 overexpression and HMOX1 knockdown (scale bar = 50 μm). (D,E) Cell survival and apoptosis analysis using CCK-8 and TUNEL assays (scale bar = 50 μm). In vivo experiments, $n = 6$ per group; *in vitro* experiments, $n = 3$ independent experiments. Relative TUNEL fluorescence intensity in H9c2 cardiomyocytes under the indicated conditions. Data are expressed as mean ± SD. ***$p < 0.001$ vs. NC. CCK-8, Cell Counting Kit-8; TUNEL, terminal deoxynucleotidyl transferase dUTP nick-end labeling.

Therapeutic Targeting of HSF1–HMOX1 Axis Attenuates Myocardial Injury In Vivo

Rats subjected to I/R received an HSF1 inhibitor (KRIBB11) or AAV9-HMOX1. KRIBB11 reduced infarct size ($p < 0.05$; Fig. 6A) and fibrosis ($p < 0.05$; Fig. 6B), while HMOX1 overexpression exacerbated the injury. Consistent with infarct reduction in Fig. 6A, Masson CVF in Fig. 6B decreased with KRIBB11 and increased with AAV9-HMOX1, aligning with cytokine shifts (Fig. 6C) and restored GPX4 (Fig. 6D), supporting attenuation of ferroptosis-associated fibrosis when the HSF1–HMOX1 axis is inhibited. These results confirm that inhibiting the HSF1–HMOX1 axis mitigates ferroptosis, inflammation, and tissue damage.

Discussion

Understanding how myocardial cells are injured under hypoxia/reoxygenation conditions is particularly im-

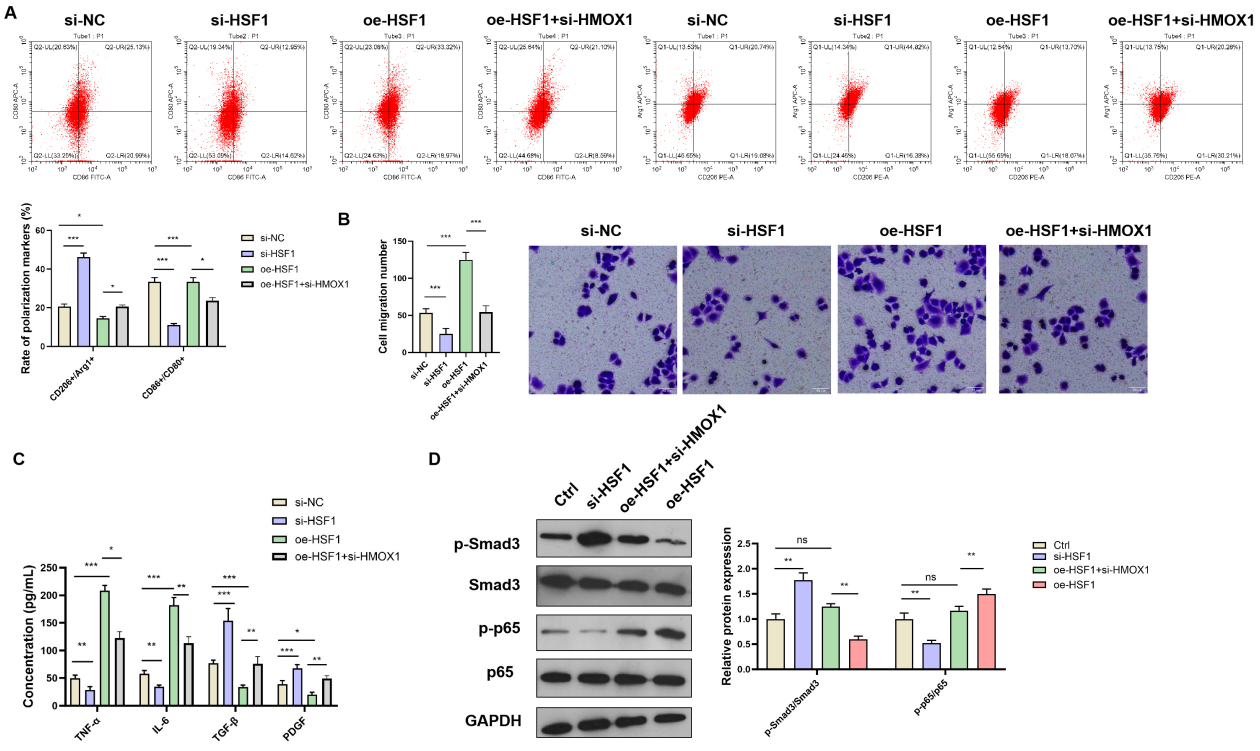

Fig. 5. The HSF1–HMOX1 axis regulates macrophage polarization by promoting ferroptosis in cardiomyocytes. (A) Flow cytometry analysis of macrophage polarization after knocking down *HSF1* and *HMOX1* genes. (B) Transwell experiments assessing the effect of conditioned medium on macrophage migration ability (scale bar = 50 μm). (C) Measurements of the levels of inflammatory factors (TNF-α, IL-6) and fibrotic factors (TGF-β, PDGF) in the co-culture system using ELISA. (D) Western blot analysis of p65/Smad activation states in macrophages. $n = 3$ independent experiments; $^{*}p < 0.05$, $^{**}p < 0.01$, $^{***}p < 0.001$. ns, not significant. PDGF, platelet-derived growth factor.

portant in cardiovascular disease research. Myocardial infarction, as a major cause of death across the spectrum of heart-related diseases, is closely tied to hypoxia and reoxygenation. Hypoxia-induced death of myocardial cells is closely associated with inflammatory responses, among which ferroptosis, as a novel form of cell death, is gradually gaining attention [14]. Studies have found that hypoxia-induced myocardial cell injury not only affects cardiac function but might also worsen inflammation by affecting how macrophages polarize, further aggravating the pathological process of MIRI [15].

This study aims to explore how the HSF1–HMOX1 signaling pathway affects ferroptosis in H9C2 myocardial cells and M1 polarization in macrophages under hypoxia/reoxygenation conditions. Through cell culture, Western blot analysis, and qPCR, we found that HSF1 and HMOX1 levels surged after hypoxia/reoxygenation, and this increase was associated with ferroptosis in myocardial cells and M1 polarization of macrophages. Our results suggest that the HSF1–HMOX1 pathway is crucial for the survival and death of myocardial cells, providing a new molecular basis for the mechanisms of MIRI.

HMOX1, or heme oxygenase-1, is a key component in ferroptosis regulation, and its expression level directly affects iron metabolism, lipid peroxidation, and oxidative stress. Several studies have shown that HMOX1 triggers ferroptosis by degrading heme and releasing free iron, as seen in acute compartment syndrome, sickle cell disease cardiomyopathy, and atherosclerosis. In acute compartment syndrome, the elevated levels of HMOX1 lead to iron overload and lipid peroxidation, thereby activating the ferroptosis pathway. Similarly, in sickle cell disease, the overexpression of HMOX1 drives ferroptosis in myocardial cells by increasing free iron and lipid peroxidation, while HMOX1 inhibitors can alleviate cardiac injury [16]. Furthermore, high levels of HMOX1 have been detected in atherosclerotic plaques and linked to macrophage ferroptosis and plaque instability [17]. These studies show that HMOX1 is a key player in ferroptosis, with its expression level directly influencing disease progression and prognosis.

HSF1 maintains redox balance within the cells and prevents apoptosis by regulating HSP70 expression in the event of hypoxic stress. Under hypoxic conditions, HIF-1α induces the *HSF1* promoter and boosts gene transcription, thereby upregulating HSP70 expression [18]. HSP70 fights off apoptosis caused by hypoxia by stabilizing mitochondrial membrane potential, regulating the Bcl-2/Bax bal-

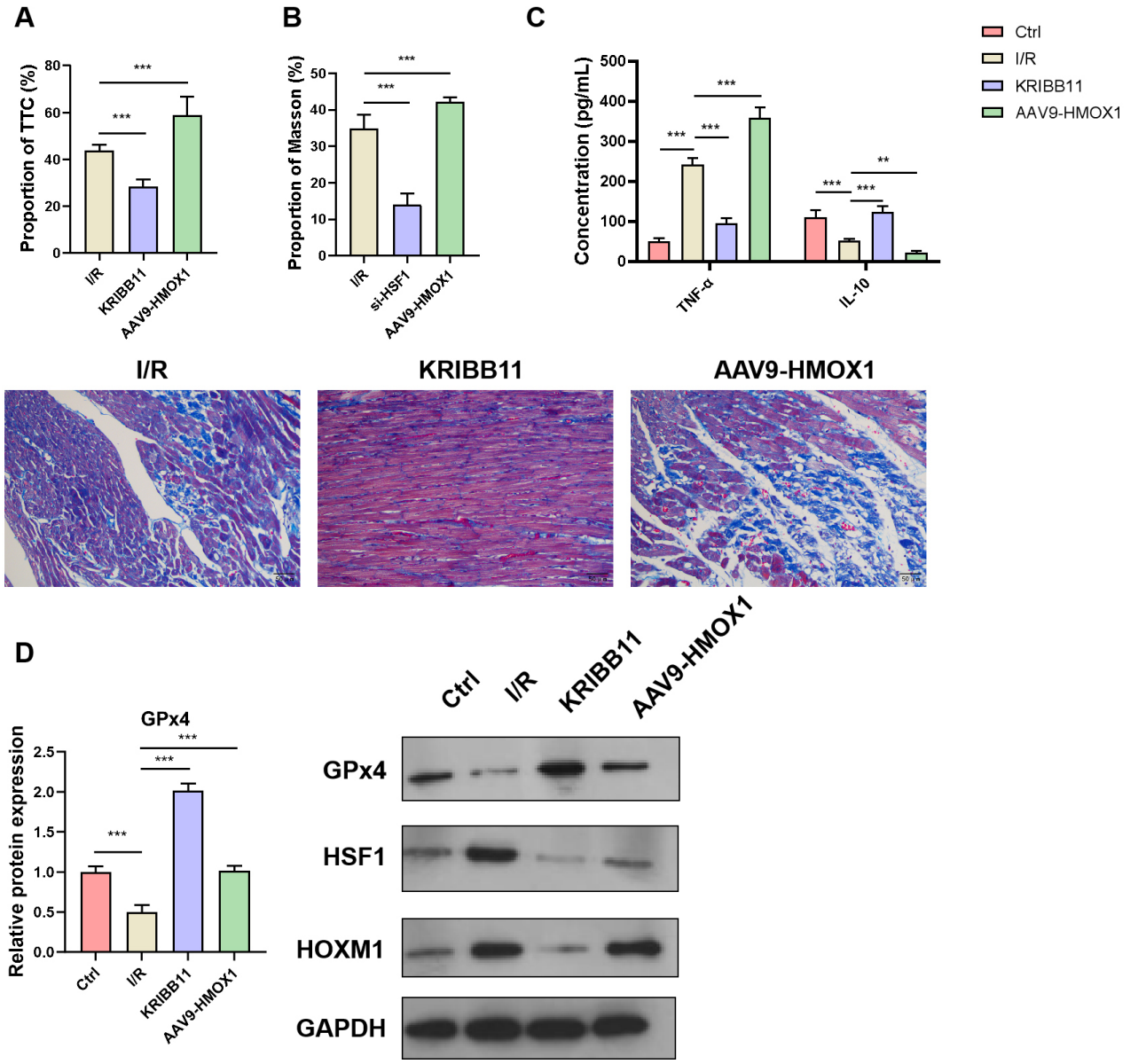

Fig. 6. Targeted intervention on the HSF1–HMOX1 axis and measurement of its impact on myocardial repair in animal models. (A) Assessment of infarct area changes via TTC staining. (B) Evaluation of myocardial fibrosis via Masson staining (scale bar = 50 μm). (C) Measurements of TNF-α and IL-10 levels using ELISA. (D) Detection of the ferroptosis protein GPX4 by means of Western blotting. *In vivo* experiments, $n = 6$ per group; *in vitro* experiments, $n = 3$ independent experiments, $^{**}p < 0.01$, $^{***}p < 0.001$.

ance, and inhibiting caspase activity [19]. Hypoxic stress not only directly causes apoptosis in myocardial cells but also exacerbates myocardial injury through various pathways, encompassing induction of endoplasmic reticulum stress, oxidative stress, and inflammatory responses [20–22]. These findings collectively point to the importance of HSF1 in myocardial infarction. HMOX1 plays a critical role in oxidative stress responses, making metabolites that have antioxidant and anti-inflammatory effects (such as carbon monoxide and biliverdin) through heme degradation. The elevation of the HMOX1 levels during I/R injury might confer protection against oxidative stress and inhibit inflammatory responses. Additionally, the expression of HMOX1 may be regulated by transcription factors such as HSF1, suggesting a possible connection between the two in the defense mechanisms against I/R injury [23]. In the present study, however, we did not perform chromatin immunoprecipitation (ChIP) or luciferase reporter assays to provide direct evidence of HSF1 binding to the *HMOX1* promoter. This limitation should be addressed in future work to confirm their regulatory relationship.

Macrophage polarization acts as a crucial player in the repair of myocardial infarction, and its dynamic balance directly affects cardiac functional recovery and prog-

nosis. Following myocardial infarction, the macrophage population in the heart tissue undergoes phenotypic alteration, gradually shifting from an early pro-inflammatory M1-dominant state to a repair M2-dominant state [24]. M1 macrophages cause deterioration of tissue damage due to the release of pro-inflammatory factors such as TNF-α and IL-6, while M2 macrophages facilitate new blood vessel formation and tissue repair by synthesizing factors like IL-10 and TGF-β [7]. It has been reported that small M2 macrophage-derived extracellular vesicles help diminish infarct size and improve cardiac function, probably through mechanisms related to miR-181b-5p–mediated glucose metabolism reprogramming and ROS inhibition. On the other hand, excessive M1 polarization may sustain inflammation and cause adverse remodeling, as monomeric C-reactive protein promotes M1 polarization through the JNK pathway, exacerbating myocardial injury [25].

In this study, we found a connection between ferroptosis and M1 polarization in macrophages. Ferroptosis in H9C2 myocardial cells promoted the polarization of macrophages toward the M1 type, thereby exacerbating the extent of myocardial infarction and providing new insights into post-ischemic inflammation, which is recognized as a significant pathophysiologic factor of myocardial infarction. Our findings highlight the interplay between myocardial cell injury and macrophage polarization, which offers new insights into novel immunotherapy strategies for improving outcomes after myocardial infarction [26,27]. With a greater understanding on the mechanism of macrophage polarization, researchers may devise a more efficient approach to preventing myocardial injury arising from hypoxia/reoxygenation, thereby improving clinical outcomes in cardiovascular diseases.

Several limitations of this study should be acknowledged. First, the study only used H9C2 myocardial cells and animal models, which might not be able to capture the complex physiology of human myocardial cells in hypoxia/reoxygenation environments. Additionally, the small sample size may limit the statistical power of the study and reduce the generalizability of the findings. More importantly, the lack of clinical validation raises questions about the reliability of translating our results to real-world settings. Therefore, future research should incorporate a wider range of cell and animal models, as well as clinical samples, to better validate the role of the HSF1–HMOX1 pathway in MIRI.

In summary, this study demonstrates how HSF1–HMOX1 expression changes under hypoxia/reoxygenation and how it significantly affects ferroptosis in cardiomyocytes and macrophage polarization. These findings provide a fresh perspective on the biological mechanisms behind myocardial infarction and may inform the development of novel therapeutic strategies. Further exploration of the HSF1–HMOX1 signaling pathway could help uncover potential targets for intervention in cardiovascular diseases.

Conclusions

In summary, the HSF1–HMOX1 axis protects against MIRI by suppressing ferroptosis and modulating inflammatory responses. Overexpression of HSF1 upregulates HMOX1, enhances antioxidant defenses, reduces cardiomyocyte death, and mitigates adverse remodeling, whereas disruption of this axis aggravates ferroptosis and myocardial injury. These findings suggest that targeting the HSF1–HMOX1 pathway may represent a promising therapeutic strategy for diminishing ischemia/reperfusion-induced cardiac damage.

Availability of Data and Materials

The datasets generated and/or analyzed during the current study are available from the corresponding author on reasonable request. Publicly available datasets used in this study include GSE254950 from the Gene Expression Omnibus (GEO, https://www.ncbi.nlm.nih.gov/geo/).

Author Contributions

ZW and LZ conceptualized and designed the study. ZW and SW carried out the experiments. SW and DG were responsible for data acquisition and statistical analysis. ZW prepared the initial draft of the manuscript. LZ, SW and DG reviewed and revised the manuscript with important intellectual input. All authors read and approved the final manuscript and agreed to be accountable for all aspects of the work.

Ethics Approval and Consent to Participate

All animal procedures were approved by the Animal Ethics Committee of The First Affiliated Hospital, Zhejiang University School of Medicine (Approval No. 20240146). All methods were performed in accordance with the relevant guidelines and regulations.

Acknowledgment

The authors would like to thank the staff of the Department of Cardiology, The First Affiliated Hospital of Zhejiang University, and Ningbo Medical Center Lihuili Hospital for their technical assistance and support.

Funding

This study was supported by the Medical Health Science and Technology Project of Zhejiang Provincial Health Commission (Grant/Award Number: 2023KY1037).

Conflict of Interest

The authors declare no conflict of interest.

Supplementary Material

Supplementary material associated with this article can be found, in the online version, at https://doi.org/10.24976/Discov.Med.202638205.36.

References

[1] Wu D, Gu Y, Zhu D. Cardioprotective effects of hydrogen sulfide in attenuating myocardial ischemia reperfusion injury (Review). Molecular Medicine Reports. 2021; 24: 875. https://doi.org/10.3892/mmr.2021.12515.

[2] Dong W, Xu H, Wei W, Ning R, Chang Y. Advances in the study of ferroptosis and its relationship to autoimmune diseases. International Immunopharmacology. 2024; 140: 112819. https://doi.org/10.1016/j.intimp.2024.112819.

[3] Han X, Zhang J, Liu J, Wang H, Du F, Zeng X, *et al*. Targeting ferroptosis: a novel insight against myocardial infarction and ischemia-reperfusion injuries. Apoptosis: An International Journal on Programmed Cell Death. 2023; 28: 108–123. https://doi.org/10.1007/s10495-022-01785-2.

[4] Zhong G, Chen J, Li Y, Han Y, Wang M, Nie Q, *et al*. Ginsenoside Rg3 attenuates myocardial ischemia/reperfusion-induced ferroptosis via the keap1/Nrf2/GPX4 signaling pathway. BMC Complementary Medicine and Therapies. 2024; 24: 247. https://doi.org/10.1186/s12906-024-04492-4.

[5] Fei Q, Ma H, Zou J, Wang W, Zhu L, Deng H, *et al*. Metformin protects against ischaemic myocardial injury by alleviating autophagy-ROS-NLRP3-mediated inflammatory response in macrophages. Journal of Molecular and Cellular Cardiology. 2020; 145: 1–13. https://doi.org/10.1016/j.yjmcc.2020.05.016.

[6] Xu S, Xu C, Xu J, Zhang K, Zhang H. Macrophage Heterogeneity and Its Impact on Myocardial Ischemia-Reperfusion Injury: An Integrative Review. Journal of Inflammation Research. 2023; 16: 5971–5987. https://doi.org/10.2147/JIR.S436560.

[7] Li Z, Ding Y, Peng Y, Yu J, Pan C, Cai Y, *et al*. Effects of IL-38 on Macrophages and Myocardial Ischemic Injury. Frontiers in Immunology. 2022; 13: 894002. https://doi.org/10.3389/fimmu.2022.894002.

[8] Sun S, Wu Y, Maimaitijiang A, Huang Q, Chen Q. Ferroptotic cardiomyocyte-derived exosomes promote cardiac macrophage M1 polarization during myocardial infarction. PeerJ. 2022; 10: e13717. https://doi.org/10.7717/peerj.13717.

[9] Jiang C, Shi Q, Yang J, Ren H, Zhang L, Chen S, *et al*. Ceria nanozyme coordination with curcumin for treatment of sepsis-induced cardiac injury by inhibiting ferroptosis and inflammation. Journal of Advanced Research. 2024; 63: 159–170. https://doi.org/10.1016/j.jare.2023.10.011.

[10] Li W, Ren Y, Meng T, Yang W, Zhang W. miR-129-5p attenuates hypoxia-induced apoptosis in rat H9c2 cardiomyocytes by activating autophagy. The Journal of Gene Medicine. 2020; 22: e3200. https://doi.org/10.1002/jgm.3200.

[11] Hensen SMM, Heldens L, van Genesen ST, Pruijn GJM, Lubsen NH. A delayed antioxidant response in heat-stressed cells expressing a non-DNA binding HSF1 mutant. Cell Stress & Chaperones. 2013; 18: 455–473. https://doi.org/10.1007/s12192-012-0400-0.

[12] Ritchie ME, Phipson B, Wu D, Hu Y, Law CW, Shi W, *et al*. limma powers differential expression analyses for RNA-sequencing and microarray studies. Nucleic Acids Research. 2015; 43: e47. https://doi.org/10.1093/nar/gkv007.

[13] Xu Z, Alloush J, Beck E, Weisleder N. A murine model of myocardial ischemia-reperfusion injury through ligation of the left anterior descending artery. Journal of Visualized Experiments: JoVE. 2014; 51329. https://doi.org/10.3791/51329.

[14] Zhang T, Han Y, Wang Y, Wang X, Zhao M, Cheng Z, *et al*. The interaction between ferroptosis and myocardial ischemia-reperfusion injury: molecular mechanisms and potential therapeutic targets. European Journal of Medical Research. 2025; 30: 643. https://doi.org/10.1186/s40001-025-02851-6.

[15] Chi H, Chai Y, Ma L, Wang Y, Wu Q, Wang L, *et al*. The mechanism by which piR-000699 targets SLC39A14 regulates ferroptosis in aging myocardial ischemia/reperfusion injury. Acta Biochimica et Biophysica Sinica. 2024; 56: 1352–1364. https://doi.org/10.3724/abbs.2024024.

[16] Menon AV, Liu J, Tsai HP, Zeng L, Yang S, Asnani A, *et al*. Excess heme upregulates heme oxygenase 1 and promotes cardiac ferroptosis in mice with sickle cell disease. Blood. 2022; 139: 936–941. https://doi.org/10.1182/blood.2020008455.

[17] Guo Z, Zhang W, Gao H, Li Y, Li X, Yang X, *et al*. High expression levels of haem oxygenase-1 promote ferroptosis in macrophage-derived foam cells and exacerbate plaque instability. Redox Biology. 2024; 76: 103345. https://doi.org/10.1016/j.redox.2024.103345.

[18] Luo SY, Wang JQ, Liu C, Gao XM, Zhang YB, Ding J, *et al*. Hif-1α/Hsf1/Hsp70 signaling pathway regulates redox homeostasis and apoptosis in large yellow croaker (*Larimichthys crocea*) under environmental hypoxia. Zoological Research. 2021; 42: 746–760. https://doi.org/10.24272/j.issn.2095-8137.2021.224.

[19] Samadi AK, Zhang X, Mukerji R, Donnelly AC, Blagg BS, Cohen MS. A novel C-terminal HSP90 inhibitor KU135 induces apoptosis and cell cycle arrest in melanoma cells. Cancer Letters. 2011; 312: 158–167. https://doi.org/10.1016/j.canlet.2011.07.031.

[20] Liu TJ, Yeh YC, Lee WL, Wang LC, Lee HW, Shiu MT, *et al*. Insulin ameliorates hypoxia-induced autophagy, endoplasmic reticular stress and apoptosis of myocardial cells: In vitro and ex vivo models. European Journal of Pharmacology. 2020; 880: 173125. https://doi.org/10.1016/j.ejphar.2020.173125.

[21] Huang S, Li Z, Jiang S, Xu M. Metabolomic study on the protective effect of isoorientin against myocardial infarction. Biochemical and Biophysical Research Communications. 2022; 598: 81–88. https://doi.org/10.1016/j.bbrc.2022.02.008.

[22] Zou H, Liu G. Inhibition of endoplasmic reticulum stress through activation of MAPK/ERK signaling pathway attenuates hypoxia-mediated cardiomyocyte damage. Journal of Receptor and Signal Transduction Research. 2021; 41: 532–537. https://doi.org/10.1080/10799893.2020.1831534.

[23] Ma D, Qiao J, Qu Q, He F, Chen W, Yu B. Weighted gene co-expression network analysis to investigate the key genes implicated in global brain ischemia/reperfusion injury in rats. Advances in Clinical and Experimental Medicine: Official Organ Wroclaw Medical University. 2020; 29: 649–659. https://doi.org/10.17219/acem/121918.

[24] Kim Y, Nurakhayev S, Nurkesh A, Zharkinbekov Z, Saparov A. Macrophage Polarization in Cardiac Tissue Repair Following Myocardial Infarction. International Journal of Molecular Sciences. 2021; 22: 2715. https://doi.org/10.3390/ijms22052715.

[25] Zha Z, Cheng Y, Cao L, Qian Y, Liu X, Guo Y, *et al*. Monomeric CRP Aggravates Myocardial Injury After Myocardial Infarction by Polarizing the Macrophage to Pro-Inflammatory Phenotype Through JNK Signaling Pathway. Journal of Inflammation Research. 2021; 14: 7053–7064. https://doi.org/10.2147/JIR.S316816.

[26] Li J, Li H, Niu N, Zhu Y, Hou S, Zhao W. NRF-1 promotes FUNDC1-mediated mitophagy as a protective mechanism against hypoxia-induced injury in cardiomyocytes. Experimental Cell Research. 2025; 446: 114472. https://doi.org/10.1016/j.yexcr.2025.114472.

[27] Nawaz S, Chinnadurai R, Al-Chalabi S, Evans P, Kalra PA, Syed AA, *et al*. Obesity and chronic kidney disease: A current review. Obesity Science & Practice. 2022; 9: 61–74. https://doi.org/10.1002/osp4.629.